Monthly Notices
of the
ROYAL ASTRONOMICAL SOCIETY

Mon. Not. R. Astron. Soc. **421,** 1764–1778 (2012) doi:10.1111/j.1365-2966.2012.20442.x

The relation between broad lines and γ-ray luminosities in *Fermi* blazars

T. Sbarrato,[1⋆] G. Ghisellini,[2] L. Maraschi[3] and M. Colpi[1]

[1]*Department of Physics G. Occhialini, University of Milano-Bicocca, Piazza della Scienza 3, I-20126 Milano, Italy*
[2]*INAF – Osservatorio Astronomico di Brera, Via Bianchi 46, I-23807 Merate, Italy*
[3]*INAF – Osservatorio Astronomico di Brera, Via Brera 28, I-20100 Milano, Italy*

Accepted 2011 December 22. Received 2011 December 21; in original form 2011 August 1

ABSTRACT

We study the relation between the mass accretion rate, the jet power and the black hole mass of blazars. With this aim, we make use of the Sloan Digital Sky Survey and the 11-month catalogue of blazars detected at energies larger than 100 MeV by the Large Area Telescope onboard the *Fermi* satellite. This allows us to construct a relatively large sample of blazars with information about both the luminosity (or upper limits) of their emission lines (used as a proxy for the strength of the disc luminosity) and the luminosity of the high-energy emission (used as a proxy for the jet power). We find a good correlation between the luminosity of the broad lines and the γ-ray luminosities as detected by *Fermi*, both using the absolute values of the luminosities and normalizing them to the Eddington value. The data we have analysed confirm that the division of blazars into BL Lacertae objects (BL Lacs) and flat spectrum radio quasars (FSRQs) is controlled by the line luminosity in Eddington units. For small values of this ratio, the object is a BL Lac, while it is a FSRQ for large values. The transition appears to be smooth, but a much larger number of objects is needed to confirm this point.

Key words: radiation mechanisms: non-thermal – BL Lacertae objects: general – quasars: general – gamma-rays: general – X-rays: general.

1 INTRODUCTION

The classic division between flat spectrum radio quasars (FSRQs) and BL Lacertae objects (BL Lacs) is mainly based on the equivalent width (EW) of the emission lines. Objects with a rest-frame EW > 5 Å are classified as FSRQs (e.g. Urry & Padovani 1995). Marcha et al. (1996) and Landt, Padovani & Giommi (2002) discussed the Ca H&K 4000-Å (rest-frame) break as a criterion to help to distinguish BL Lacs from low-luminosity radio galaxies. Furthermore, Marcha et al. (1996) proposed that objects with a weak Ca break, and with an EW even larger than 5 Å, should be classified as BL Lacs. However, Scarpa & Falomo (1997) have shown a continuity between BL Lacs and FSRQs with respect to the luminosity of the Mg II line, which can be taken as an indication that there is no clear separation of blazars into the two subclasses. Landt et al. (2004), instead, considered narrow lines, such as [O II] and [O III], and found that it is possible to separate intrinsically weak- and strong-line blazars in the [O II] and [O III] EW plane.

The classification scheme that is based on the EW of the broad lines has been adopted, both because it is observationally simple and because it was thought to measure the relative importance of the non-thermal, rather than thermal, jet emission. However, we now know that the jet electromagnetic output is often dominated by emission at higher energies (hard X-rays and γ-rays), and therefore the EW of the optical emission lines is not a good measure of the jet dominance. Furthermore, the jet flux is much more variable than the underlying thermal emission, which causes the measured EW to vary. Occasionally, a blazar with very luminous emission lines, which should be classified as a FSRQ, can instead appear as a BL Lac when the optical jet flux is particularly strong. Conversely, a BL Lac in a particular faint state could show broad emission lines that, albeit weak, can have an EW greater than 5 Å. Therefore, in an earlier paper (Ghisellini et al. 2011, hereafter G11), we proposed a more physical distinction between the two classes of blazars, based on the luminosity of the broad emission lines measured in Eddington units: $L_{\rm BLR}/L_{\rm Edd}$. We proposed that the objects are FSRQs when $L_{\rm BLR}/L_{\rm Edd} \gtrsim 5 \times 10^{-4}$, and that they are BL Lacs below this value. Normalizing to the Eddington luminosity ensures the appropriate comparison among objects of different black hole masses.

The sample of blazars studied in G11 was limited, because it was based both on a small subsample of bright FSRQs detected in γ-rays by the *Fermi* satellite during the first three months of operation, the *Fermi* All-Sky Survey (LBAS sample; Abdo et al. 2009), and on BL Lacs detected by *Fermi* during the first 11 months, the First Large Area Telescope (LAT) Active Galactic Nuclei (AGNs) Catalogue (1LAC sample; Abdo et al. 2010a), with a relatively steep γ-ray energy spectral index α_γ ($\alpha_\gamma > 1.2$). These BL Lacs occupy

⋆E-mail: tullia.sbarrato@brera.inaf.it

the region of the spectral index–γ-ray luminosity (α_γ–L_γ) plane occupied mainly by FSRQs (see Ghisellini, Maraschi & Tavecchio 2009).

Because the broad emission lines are produced by clouds that are photoionized by the radiation produced by the accretion disc, there is a direct relation between $L_{\rm BLR}$ and the accretion disc luminosity $L_{\rm d}$. Therefore, by measuring the broad line luminosities, we gather information on the disc luminosity even when it is not directly visible, as often occurs in blazars whose optical continuum is dominated by the jet flux. In turn, by knowing $L_{\rm BLR}$ and the bolometric jet luminosity, we can then study the relation between the jet and the accretion power. In fact, this is the final aim of these studies. Earlier attempts to find the ratio between the jet and the accretion power have been made by, for example, Celotti, Padovani & Ghisellini (1997) and by D'Elia, Padovani & Landt (2003). Here, the novelty is, on the one hand, the method used to estimate the jet power and, on the other hand, the large number of sources for which the γ-ray detection ensures a good estimate of the jet power (or at least a good proxy for it), coupled with the large number of blazars present in the Sloan Digital Sky Survey (SDSS; York et al. 2000) with spectroscopic data.

Another important element in this line of research is the black hole mass, which allows us to measure the luminosities and powers in Eddington units. Besides allowing us to compare objects with different black hole masses, it allows us to investigate whether the accretion regime has a transition, from radiatively efficient to inefficient, when the mass accretion rate in Eddington units $\dot{M}/\dot{M}_{\rm Edd}$ goes below a critical value (e.g. Narayan, Garcia & McClintock 1997). It also allows us to see how this influences the jet power. For instance, the division between BL Lacs and FSRQs in the sample of blazars detected during the first three months of the *Fermi* All-Sky Survey (LBAS) seems to corresponds to disc luminosities $L_{\rm d}/L_{\rm Edd} \sim 10^{-2}$ (Ghisellini et al. 2009); see also the earlier proposal about the division of Fanaroff–Riley type I and type II (FR I and II) radio galaxies in Ghisellini & Celotti (2001).

For these reasons, we are motivated to enlarge the original sample of G11, studying all blazars for which we have information about their emission lines (as a proxy for the disc luminosity), their γ-ray luminosity (as a proxy for the jet power) and their black hole mass. The two largest samples useful for this study are the SDSS and the *Fermi* 1LAC sample. In Section 2, we present the samples used for this work, and in Section 3 we discuss how we have derived the broad line luminosities, or their upper limits. In Section 4, we present the relation between $L_{\rm BLR}$ and the γ-ray luminosities, and we discuss our findings in Section 5.

2 SAMPLES

We are interested in grouping a large number of blazars with reliable measures of the broad line region (BLR) and γ-ray luminosities. The SDSS, which provides the largest publicly available catalogue of spectral objects, and the LAT onboard the *Fermi Gamma-Ray Space Telescope* are the optimal devices for this investigation.

For our analysis, we have tried to select the largest group of blazars with reliable measurements of redshift and black hole mass. First, we grouped a sample of optically selected quasars from the SDSS (seventh data release, DR7), which have been analysed in depth by Shen et al. (2011, hereafter S11) and have been detected by *Fermi*. Furthermore, in order to extend our analysis towards lower luminosities, we have included an optically selected group of BL Lac candidates. The BL Lacs that we have taken into consideration are supposed to be lineless, but their redshift and black hole masses have been derived by Plotkin et al. (2011, hereafter P11) from the galaxy spectral absorption features. Finally, we have tried to look for possible intermediate objects, which have been excluded from both the SDSS DR7 quasar catalogue and the BL Lacs catalogue of P11. For this purpose, we have selected a small group of AGNs from the previous SDSS data release (DR6; Adelman-McCarthy et al. 2008), which have been detected by *Fermi*.

2.1 1LAC sample

The 1LAC sample is the AGN sample that resulted from 11 months of operation of the LAT onboard the *Fermi* satellite (Abdo et al. 2010a). As revised in Ackermann et al. (2012), this sample consists of 671 sources at high Galactic latitude ($|b| > 10^\circ$). The statistical significance of the *Fermi* detection was required to be TS > 25, where TS stands for test statistics; see Mattox et al. (1996) for the definition (TS $= 25$ approximately corresponds to 5σ).

By requiring that the associations of the detected sources have a probability $P \geq 80$ per cent and that there is only one AGN in the positional error box of the *Fermi* detection, the *Fermi* team has constructed a clean 1LAC sample, composed of 599 AGNs. Of these, 248 are classified by the *Fermi*/LAT team as FSRQs and 275 as BL Lacs. The remaining sources either are of unknown blazar type (50) or are non-blazar AGNs (26). We focus on the 248 FSRQs and 275 BL Lacs. All FSRQs have known redshifts; for about half of the BL Lacs, the redshift is still unknown.

2.2 SDSS DR7 quasar sample

First, we collected a group of optically selected quasars. The SDSS provides a quasar catalogue from the DR7, which includes 105 783 objects and has been spectrally analysed by S11. This sample includes quasars that have luminosities larger than $M_i = -22$ [i.e. $\nu L_\nu(5100\ \text{Å}) = 10^{44}$ erg s^{-1}], that have at least one emission line with FWHM > 1000 km s^{-1} and that have a reliable spectroscopical redshift. For this group of sources, S11 calculated the continuum and emission-line measurements around the Hα, Hβ, Mg II and C IV regions. They derived the virial black hole masses with different calibrations, along with what they considered to be the best estimate. The broad line luminosities and the best estimates of the black hole masses are considered for our work.

From the cross-correlation with the 1LAC sample, we obtained a group of 49 *Fermi*-detected and optically selected quasars. We have excluded three objects for which S11 have not provided a reliable estimate of the black hole mass. Therefore, the quasar sample under study includes 46 objects, and these are listed in Table 1. Note that because we require that the objects have a broad emission line with measurable FWHM, BL Lacs with very weak or no emission lines are automatically excluded.

2.3 BL Lac sample of P11

In our analysis, we have included all the optically selected BL Lacs that are present in P11. In their work, P11 start from an original sample of 723 BL Lac candidates with EW < 5 Å, which are included in the DR7 general catalogue (for selection details, see Plotkin et al. 2010). From this original sample, they selected 143 BL Lac candidates that have a reliable redshift limited to $z < 0.4$, that are radio-loud and that match to a radio source from the Faint Images of the Radio Sky at 20 cm survey (FIRST; White et al. 1997) and/or the National Radio Astronomy Observatories Very Large Array Sky Survey (NVSS; Condon et al. 1998). Then, they

Table 1. Sources from the SDSS DR7 quasar catalogue that are present in the 1LAC *Fermi* sample. The columns give the following: (1) name; (2) right ascension; (3) declination; (4) redshift; (5) logarithm of the black hole mass (in solar masses, with the best estimate from S11); (6) lines measured by S11, from which $L_{\rm BLR}$ has been derived; (7) BLR luminosity (10^{42} erg s^{-1}), obtained from the line luminosities calculated by S11; (8) γ-ray luminosity from *Fermi* data (10^{45} erg s^{-1}), averaged over the first 11 months of the *Fermi* operations.

Name	RA	Dec.	z	$\log M\,{\rm M}_\odot^{-1}$	Lines	$L_{\rm BLR}$ (10^{42} erg s^{-1})	L_γ (10^{45} erg s^{-1})
(1)	(2)	(3)	(4)	(5)	(6)	(7)	(8)
CGRaBS J0011+0057	00 11 30.40	+00 57 51.7	1.493	8.95	Mg II	472.91	217.51
B3 0307+380	03 10 49.87	+38 14 53.8	0.816	8.23	Hβ Mg II	65.97	54.97
B2 0743+25	07 46 25.87	+25 49 02.1	2.978	9.59	C IV	4199.17	3849.95
OJ 535	08 24 47.24	+55 52 42.6	1.418	9.42	Mg II	2004.82	643.44
B2 0827+24	08 30 52.08	+24 10 59.8	0.941	9.01	Mg II	974.10	227.73
PKS 0906+01	09 09 10.09	+01 21 35.6	1.025	9.32	Mg II	1883.33	462.35
0917+444	09 20 58.46	+44 41 54.0	2.188	9.25	Mg II C IV	7075.62	8261.87
0917+62	09 21 36.23	+62 15 52.1	1.453	9.37	Mg II	978.32	349.93
B2 0920+28	09 23 51.52	+28 15 25.1	0.744	8.80	Hβ Mg II	257.91	52.06
CGRaBS J0937+5008	09 37 12.32	+50 08 52.1	0.275	8.29	Hα Hβ	18.18	4.59
CGRaBS J0941+2728	09 41 48.11	+27 28 38.8	1.306	8.68	Mg II	4843.97	119.81
CRATES J0946+1017	09 46 35.06	+10 17 06.1	1.005	8.52	Mg II	639.52	91.52
CGRaBS J0948+0022	09 48 57.31	+00 22 25.5	0.584	7.77	Hβ Mg II	126.83	101.32
B2 0954+25A	09 56 49.87	+25 15 16.0	0.708	9.34	Hβ Mg II	789.15	32.10
4C +55.17	09 57 38.18	+55 22 57.7	0.899	8.96	Mg II	374.96	453.58
CRATES J1016+0513	10 16 03.13	+05 13 02.3	1.713	9.11	Mg II C IV	463.36	2002.10
B3 1030+415	10 33 03.70	+41 16 06.2	1.116	8.65	Mg II	857.50	145.07
CRATES J1112+3446	11 12 38.77	+34 46 39.0	1.955	9.04	Mg II C IV	2108.88	583.93
CRATES J1117+2014	11 17 06.25	+20 14 07.3	0.137	8.62	*Hα* Hβ	1.37	1.14
B2 1144+40	11 46 58.29	+39 58 34.2	1.088	8.98	Mg II	1171.13	124.91
4C +29.45	11 59 31.83	+29 14 43.8	0.724	9.18	Hβ Mg II	513.10	196.10
CRATES J1208+5441	12 08 54.24	+54 41 58.1	1.344	8.67	Mg II	321.88	333.08
CRATES J1209+1810	12 09 51.76	+18 10 06.8	0.850	8.94	Hβ Mg II	288.94	40.69
4C +04.42	12 22 22.55	+04 13 15.7	0.965	8.24	Mg II	720.10	169.22
4C +21.35	12 24 54.46	+21 22 46.3	0.433	8.87	Hβ Mg II	1617.49	29.89
CRATES J1228+4858	12 28 51.76	+48 58 01.2	1.722	9.22	Mg II C IV	585.70	468.20
CRATES J1239+0443	12 39 32.75	+04 43 05.3	1.760	8.67	Mg II C IV	912.84	1418.40
B2 1255+32	12 57 57.23	+32 29 29.2	0.805	8.74	Hβ Mg II	349.38	27.59
B2 1308+32	13 10 28.66	+32 20 43.7	0.997	8.80	Mg II	837.76	497.26
B2 1315+34A	13 17 36.49	+34 25 15.8	1.054	9.29	Mg II	1175.14	55.36
CGRaBS J1321+2216	13 21 11.20	+22 16 12.1	0.948	8.42	Mg II	272.05	58.82
B2 1324+22	13 27 00.86	+22 10 50.1	1.403	9.24	Mg II	786.65	519.85
B3 1330+476	13 32 45.23	+47 22 22.6	0.669	8.56	Hβ Mg II	256.41	18.89
B2 1348+30B	13 50 52.73	+30 34 53.5	0.712	8.69	Hβ Mg II	211.68	22.73
PKS 1434+235	14 36 40.98	+23 21 03.2	1.547	8.44	Mg II C IV	595.91	110.86
PKS 1502+106	15 04 24.98	+10 29 39.1	1.839	9.64	Mg II C IV	1983.07	22563.8
PKS 1509+022	15 12 15.74	+02 03 16.9	0.219	8.84	Hα Hβ	10.56	3.98
PKS 1546+027	15 49 29.43	+02 37 01.1	0.414	8.61	Hβ Mg II	821.22	22.16
4C +05.64	15 50 35.27	+05 27 10.4	1.417	9.38	Mg II	1138.94	209.33
PKS 1551+130	15 53 32.69	+12 56 51.7	1.308	9.10	Mg II	1587.17	1003.15
4C +10.45	16 08 46.20	+10 29 07.7	1.231	8.64	Mg II	1014.70	361.88
B2 1611+34	16 13 41.06	+34 12 47.8	1.399	9.12	Mg II	3131.09	95.51
CRATES J1616+4632	16 16 03.77	+46 32 25.2	0.950	8.44	Mg II	233.23	93.91
4C +38.41	16 35 15.49	+38 08 04.4	1.813	9.53	Mg II C IV	5743.01	3420.04
CRATES J2118+0013	21 18 17.39	+00 13 16.7	0.462	7.93	Hβ Mg II	114.78	6.23
PKS 2227−08	22 29 40.08	−08 32 54.4	1.559	8.95	Mg II C IV	4613.63	2464.28

applied a spectral decomposition in order to separate the galaxy and AGN spectral components. Only 71 out of the 143 BL Lacs could be successfully decomposed. For this smaller sample of 71 BL Lacs, the black hole masses were derived from the M–σ_* relation.

A similar study on the black hole masses of SDSS BL Lacs has been carried out by León-Tavares et al. (2011). They started from a sample of BL Lacs included in the SDSS Data Release 5 (DR5) and radio-detected by FIRST. This original BL Lac sample was selected by Plotkin et al. (2008). León-Tavares et al. (2011) performed a spectral decomposition similar to that in P11 on objects in the redshift range $0.06 < z < 0.5$. They obtained estimates of the black hole masses for 78 BL Lacs, using the M–σ_* relation. The results of León-Tavares et al. (2011) and P11 are very similar and the two works are consistent. We have decided to use the P11 data.

We cross-correlated the P11 sample with the clean 1LAC sample. We found that 10 out of the 71 BL Lacs have been detected by *Fermi*, and hence we have measurements of their γ-ray luminosities. For the other 61 sources, we derived an upper limit on their γ-ray fluxes,

based on the sensitivity limit of the LAT for objects with $\Gamma_\gamma \simeq 2$. Therefore, the upper limit in flux for these 61 BL Lacs is fixed at $F_{\rm ph} = 5 \times 10^{-9}$ ph cm^{-2} s^{-1}. The overall BL Lac sample under study includes 71 objects, which are listed in Table 2.

2.4 SDSS DR6 sample

We selected a final group of sources from the SDSS Data Release 6 (DR6), in order to include in our analysis possible optically intermediate objects, which might have been excluded from the S11 and P11 catalogues. Therefore, we cross-correlated the SDSS DR6 and the clean 1LAC, and we obtained a group of 20 additional sources that are not contained in the samples mentioned above. Three of these sources have no reliable redshifts, and we have excluded these from our sample. Because we do not have estimates of the black hole masses for this group of sources, we have chosen to assign them an average value of $M = 5 \times 10^8$ M$_\odot$. This last group of intermediate blazars includes 17 objects, which are listed in Table 3.

In summary, the sample that we study is composed of the following.

(i) 46 *Fermi*-detected, optically selected FSRQs from S11. These objects have detections on both $L_{\rm BLR}$ and L_γ, and have black hole masses estimated by S11.

(ii) 10 *Fermi*-detected, optically selected BL Lacs from P11. Because of their original selection, these sources do not show any emission line. Therefore, we have calculated the upper limit on $L_{\rm BLR}$, while detections are available for L_γ. The 1LAC catalogue provides an upper limit instead of a detection for one of these sources. P11 provide mass estimates for all these objects.

Table 2. BL Lacs from the work by P11. The columns give the following: (1) SDSS name; (2) redshift; (3) logarithm of the black hole mass (in solar masses; P11); (4) lines from which we derived the upper limits, as described in Section 3.1; (5) the upper limit on the BLR luminosity (10^{42} erg s^{-1}), obtained from the upper limit on line fluxes; (6) the upper limit on the γ-ray luminosity obtained from the *Fermi*/LAT sensitivity limit, in units of 10^{44} erg s^{-1}; (7) γ-ray luminosity from *Fermi* data (10^{44} erg s^{-1}), averaged over the first 11 months of the *Fermi* operations.

Name (SDSS J...)	z	$\log M\,{\rm M}_\odot^{-1}$	Lines	UL $L_{\rm BLR}$ (10^{42} erg s^{-1})	UL L_γ (10^{44} erg s^{-1})	L_γ (10^{44} erg s^{-1})
(1)	(2)	(3)	(4)	(5)	(6)	(7)
002200.95 +000657.9	0.306	8.49	Hα Hβ	3.65	1.07	
005620.07 −093629.7	0.103	9.01	Hα Hβ	1.02	0.95	
075437.07 +391047.7	0.096	8.24	Hα Hβ	0.52	0.81	
080018.79 +164557.1	0.309	8.58	Hα Hβ	5.68	1.09	
082323.24 +152447.9	0.167	8.80	Hα Hβ	1.62	2.69	
082814.20 +415351.9	0.226	8.83	Hα Hβ	2.55	5.24	
083417.58 +182501.6	0.336	9.34	Hβ	5.79	13.18	
083548.14 +151717.0	0.168	7.94	Hα Hβ	2.87	2.75	
083918.74 +361856.1	0.335	8.50	Hβ	7.89	13.18	
084712.93 +113350.2	0.198	8.52	Hα Hβ	3.38		3.34
085036.20 +345522.6	0.145	8.61	Hα Hβ	2.07		1.74
085729.78 +062725.0	0.338	8.23	Hβ	7.23	13.48	
085749.80 +013530.3	0.281	8.69	Hα Hβ	5.85	8.70	
090207.95 +454433.0	0.289	8.78	Hα Hβ	5.24	9.33	
090314.70 +405559.8	0.188	8.28	Hα Hβ	2.02	3.54	
090953.28 +310603.1	0.272	8.95	Hα Hβ	6.54	8.12	
091045.30 +254812.8	0.384	8.51	Hβ	9.92	18.19	
091651.94 +523828.3	0.190	8.53	Hα Hβ	3.07	3.63	
093037.57 +495025.6	0.187	8.48	Hα Hβ	3.26	3.46	
094022.44 +614826.1	0.211	8.57	Hα Hβ	3.55		11.57
094542.23 +575747.7	0.229	8.63	Hα Hβ	3.23		15.97
101244.30 +422957.0	0.365	8.67	Hβ	13.30	15.84	
102453.63 +233234.0	0.165	7.46	Hα Hβ	2.68	2.63	
102523.04 +040228.9	0.208	8.18	Hα Hβ	2.74	4.36	
103317.94 +422236.3	0.211	8.59	Hα Hβ	3.18	4.57	
104029.01 +094754.2	0.304	8.70	Hα Hβ	6.45	10.47	
104149.15 +390119.5	0.208	8.55	Hα Hβ	3.23	4.36	
104255.44 +151314.9	0.307	7.81	Hα Hβ	4.56	10.71	
105344.12 +492955.9	0.140	8.47	Hα Hβ	1.68		3.03
105538.62 +305251.0	0.243	8.43	Hα Hβ	4.10	6.30	
105606.61 +025213.4	0.236	8.11	Hα Hβ	3.43	5.88	
105723.09 +230318.7	0.378	8.32	Hβ	9.91	17.37	
112059.74 +014456.9	0.368	9.60	Hβ	9.81	16.21	
113630.09 +673704.3	0.134	8.30	Hα Hβ	1.07		2.03
114023.48 +152809.7	0.244	9.46	Hα Hβ	4.43	6.30	
114535.10 −034001.4	0.168	8.27	Hα Hβ	2.08	2.75	
115404.55 −001009.8	0.254	8.36	Hα Hβ	3.54		5.53
115709.53 +282200.7	0.300	9.20	Hα Hβ	5.60	10.23	

Table 2 – *continued*

Name (SDSS J...)	z	$\log M\ M_{\odot}^{-1}$	Lines	UL $L_{\rm BLR}$ (10^{42} erg s^{-1})	UL L_{γ} (10^{44} erg s^{-1})	L_{γ} (10^{44} erg s^{-1})
(1)	(2)	(3)	(4)	(5)	(6)	(7)
120837.27 +115937.9	0.369	8.66	Hβ	12.56	16.21	
123123.90 +142124.4	0.256	8.62	Hα Hβ	5.37	7.07	
123131.39 +641418.2	0.163	8.84	Hα Hβ	1.96	2.57	
123831.24 +540651.8	0.224	8.61	Hα Hβ	4.15	5.24	
125300.95 +382625.7	0.371	8.24	Hβ	6.81	16.59	
131330.12 +020105.9	0.356	8.50	Hβ	8.05	15.13	
132231.46 +134429.8	0.377	8.97	Hβ	9.92	17.37	
132239.31 +494336.2	0.332	8.67	Hβ	7.66	12.88	
132301.00 +043951.3	0.224	8.86	Hα Hβ	4.23	5.24	
132617.70 +122958.7	0.204	8.63	Hα Hβ	3.66	4.16	
133612.16 +231958.0	0.267	8.56	Hα Hβ	4.70	7.76	
134105.10 +395945.4	0.172	8.48	Hα Hβ	2.79	10.12[a]	
134136.23 +551437.9	0.207	8.29	Hα Hβ	3.68	4.36	
134633.98 +244058.4	0.167	8.29	Hα Hβ	2.42	2.69	
135314.08 +374113.9	0.216	8.79	Hα Hβ	3.66	4.78	
140350.28 +243304.8	0.343	8.39	Hβ	7.44	13.80	
142421.17 +370552.8	0.290	8.39	Hα Hβ	5.34	9.33	
142832.60 +424021.0	0.129	8.70	Hα Hβ	1.90		1.86
144248.28 +120040.2	0.163	8.94	Hα Hβ	2.46		3.45
144932.70 +274621.6	0.227	8.86	Hα Hβ	3.77	5.37	
153311.25 +185429.1	0.307	8.91	Hα Hβ	6.45	10.71	
155412.07 +241426.6	0.301	8.59	Hα Hβ	5.00	10.23	
155424.12 +201125.4	0.222	8.94	Hα Hβ	3.66	5.12	
160118.96 +063136.0	0.358	8.69	Hβ	6.78	15.13	
160519.04 +542059.9	0.212	7.85	Hα Hβ	3.28	4.57	
161541.21 +471111.7	0.199	8.17	Hα Hβ	3.92	3.98	
161706.32 +410647.0	0.267	7.84	Hα Hβ	6.22	7.76	
162839.03 +252755.9	0.220	8.90	Hα Hβ	2.71	5.01	
163726.66 +454749.0	0.192	8.42	Hα Hβ	3.07	3.71	
164419.97 +454644.3	0.225	8.76	Hα Hβ	4.64	5.24	
205456.85 +001537.7	0.151	8.67	Hα Hβ	1.49	2.18	
205938.57 −003756.0	0.335	7.16	Hβ	6.61	13.18	
223301.11 +133602.0	0.214	8.54	Hα Hβ	3.02	4.67	

[a] The upper limit is from the list of Abdo et al. (2010a).

(iii) 61 optically selected BL Lacs from P11 that are not *Fermi*-detected. As for the other 10 sources from P11, they have mass estimates (from P11) and upper limits on $L_{\rm BLR}$. However, in addition, we have also calculated the upper limits on L_{γ}.

(iv) 14 *Fermi*-detected objects that are included in the DR6 general sample. These objects do not show broad emission lines in their spectra, and hence we have calculated the upper limits on their $L_{\rm BLR}$. In SDSS DR6, there are no estimates of the black hole mass, and hence we have assigned to these objects an average mass value ($M = 5 \times 10^8\ M_{\odot}$).

(v) Three *Fermi*-detected blazars that are included in the DR6 sample. These objects show at least one emission line in their spectra, and hence they have detections on both $L_{\rm BLR}$ and L_{γ}. For one of these, we have calculated a mass estimate from the FWHM of the Hβ line, while we assigned to the others an average mass value.

In total, we have 49 objects with detections on both $L_{\rm BLR}$ and L_{γ}, 23 objects with upper limits on $L_{\rm BLR}$ and detections on L_{γ} and 62 objects with upper limits on both luminosities. In the following, when discussing the relation between the BLR and the γ-ray luminosity, we add to our sample other 30 blazars studied in G11, which are listed in Table 4. Of these 30 objects, 14 are FSRQs and 16 are BL Lacs; these 16 BL Lacs include 12 low-frequency peaked BL Lacs (LBLs) and four high-frequency peaked BL Lacs (HBLs). Also, 29 objects have measured $L_{\rm BLR}$ and γ-ray detections, while one has an upper limit on $L_{\rm BLR}$ and a γ-ray detection. Therefore, there are a total of 78 blazars with measured $L_{\rm BLR}$, L_{γ} and black hole mass.

3 BROAD LINE LUMINOSITIES

We have taken the luminosity of the emission lines of the blazars in the SDSS DR7 quasar sample directly from the values listed in the S11 catalogue. In order to calculate the total luminosity of the broad lines, we have followed Celotti et al. (1997). Specifically, we have set the Lyα flux contribution to 100, and the relative weights of the Hα, Hβ, Mg II and C IV lines to 77, 22, 34 and 63, respectively (see Francis et al. 1991). The total broad line flux is fixed at 555.76. The $L_{\rm BLR}$ value or the upper limit of each source has been derived using these proportions. We list these blazars in Table 1, reporting the type of line used for calculating $L_{\rm BLR}$ and the values of the estimated $L_{\rm BLR}$ and the observed L_{γ}. When more than one line is present, we calculate the simple average of the $L_{\rm BLR}$ estimated from each line.

3.1 Upper limits on the broad line luminosity

While the SDSS DR7 quasar sample is selected because it contains spectra with prominent broad emission lines, which have been measured by S11, the other two samples include mostly lineless

Table 3. Sources from the SDSS DR6 catalogue that are present in the 1LAC *Fermi* sample. The columns give the following: (1) name; (2) right ascension; (3) declination; (4) redshift; (5) lines measured or for which we derived the upper limits as described in Section 3.1; (6) the upper limit on the BLR luminosity (10^{42} erg s^{-1}), obtained from the UL on line fluxes; (7) luminosity of the BLR (10^{42} erg s^{-1}); (8) γ-ray luminosity from *Fermi* data (10^{45} erg s^{-1}), averaged on the first 11 months of the *Fermi* operations. The black hole masses are not available, so a medium mass value ($M = 5 \times 10^8$ M$_\odot$) has been assigned to all of them.

Name	RA	Dec.	z	Lines	UL $L_{\rm BLR}$ (10^{42} erg s^{-1})	$L_{\rm BLR}$ (10^{42} erg s^{-1})	L_γ (10^{45} erg s^{-1})
(1)	(2)	(3)	(4)	(5)	(6)	(7)	(8)
B2 0806+35	08 09 38.87	+34 55 37.2	0.082	Hα Hβ	0.49		0.18
CRATES J0809+5218	08 09 49.18	+52 18 58.2	0.138	Hα Hβ	7.581		1.45
Ton 1015	09 10 37.03	+33 29 24.4	0.354	Hα Hβ	30.675		4.54
CRATES J1012+0630	10 12 13.34	+06 30 57.2	0.727	Hβ Mg II	134.295		35.9
1ES 1011+496	10 15 04.14	+49 26 00.6	0.212	Hβ	19.9		9.72
B2 1040+24A	10 43 09.04	+24 08 35.4	0.560	Mg II		25.4	13.7
PKS 1055+01	10 58 29.60	+01 33 58.8	0.890	Mg II		131.8	377.2
CGRaBS J1058+5628	10 58 37.73	+56 28 11.1	0.143	Hα Hβ	3.85		3.58
PKS 1106+023[a]	11 08 45.48	+02 02 40.8	0.157	Hβ		4.7	0.51
1ES 1118+424	11 20 48.06	+42 12 12.4	0.124	Hα Hβ	1.797		0.47
B2 1147+24	11 50 19.21	+24 17 53.8	0.200	Hα Hβ	9.627		1.47
B2 1218+30	12 21 21.94	+30 10 37.2	0.184	Hα Hβ	6.04		3.34
W Com	12 21 31.69	+28 13 58.4	0.102	Hα Hβ	5.26		1.80
B2 1229+29	12 31 43.57	+28 47 49.7	0.236	Hα Hβ	9.696		4.31
CRATES J1253+0326	12 53 47.00	+03 26 30.3	0.066	Hα Hβ	0.41		0.13
PG 1437+398	14 39 17.47	+39 32 42.8	0.344	Hα Hβ	17.93		4.27

[a] PKS 1106+023 has the Hβ line measured in the SDSS DR6 catalogue, so its mass can be estimated by the Chiaberge & Marconi (2011) relation: a value of $M = 4 \times 10^7$ M$_\odot$ is obtained.

objects. In these cases, we need to derive the upper limits on the line fluxes (UL$_{F_{\rm line}}$).

With this aim, the observed spectrum has been fitted with a power-law model, with the addition of possible absorption or narrow emission features modelled as Gaussian profiles. Absorption lines are clearly visible in the spectra included in P11 BL Lac sample and P11 also provide the variance of each absorption feature (σ_*). Such a modelling includes the lineless power law and the narrow features. The broad emission line for which we want to obtain the upper limit is treated as an additional Gaussian profile, with a variable flux value $F_{\rm line}$ and a FWHM fixed at the average value $v_{\rm FWHM} = 4000$ km s^{-1}, as suggested in Decarli, Dotti & Treves (2011). This value is an average for all blazars, and it is consistent with the median FWHM values that can be obtained from the whole SDSS quasar sample. Even though, in the case of BL Lacs, the average value is possibly slightly smaller, we prefer to maintain a larger average FWHM value in order to derive more conservative (i.e. less stringent) upper limits. To define the UL$_{F_{\rm line}}$, we perform a χ^2 test, varying the $F_{\rm line}$ value until our model returns an unacceptable fit. Then, we define the upper limit on the line flux as the $F_{\rm line}$ for which we obtain $\chi^2 > \chi^2$ (99 per cent). Over this critical value, the model is no longer acceptable to fit the data, and we should actually see a broad line emerging over the continuum, if present. In order to derive meaningful upper limits, we require a signal-to-noise ratio S/N > 5 in the wavelength interval in which we performed our analysis. Hence, we checked the signal-to-noise ratios of the spectra in our sample, and we excluded B3 1432+422 (SDSS J143405.69+420316.0, from the DR6 sample), because its signal-to-noise ratio was S/N < 5 over the whole spectrum. Therefore, we were left with 16 DR6 objects, as listed in Table 3.

In principle, the process used to derive the upper limits could be applied to the four lines measured in the work by S11 (i.e. Hα, Hβ, Mg II and C IV). The objects included in the P11 sample all have $z < 0.4$, and hence the UL$_{F_{\rm line}}$ can be derived only for the Hα and Hβ lines. We derive the upper limits for these two lines. We have also applied the procedure to the low-redshift objects included in the DR6 sample. For three objects from this sample, the redshift is sufficiently large to derive the upper limit on the Mg II line.

3.2 Distribution of black hole masses

As a byproduct of our study, we have collected (from the S11 and P11 samples) a large number of estimates for the black hole masses in both FSRQs and BL Lacs. FSRQs show a distribution skewed towards larger masses than BL Lacs (i.e. $\langle \log M_{\rm FSRQ} \rangle = 8.88 \pm 0.40$ and $\langle \log M_{\rm BL\,Lac} \rangle = 8.57 \pm 0.37$), while the average of all masses is $\langle \log M_{\rm all} \rangle = 8.70 \pm 0.41$. We believe that, at least in part, this is the result of a selection effect, because most BL Lacs come from the P11 sample, and therefore they have been selected to be at $z < 0.4$. Assuming that very large black hole masses are rarer than smaller ones, the largest masses are expected to be found only when considering relatively large redshifts. This is illustrated by Fig. 1, which shows the black hole masses as a function of redshift for BL Lacs and FSRQs. Apart from a few exceptions, the BL Lacs extend to $z \sim 0.4$ (by construction, given the redshift limit of the P11 sample), while the FSRQs cluster around $z \sim 1$.

4 $L_{\rm BLR}$–L_γ RELATION

Fig. 2 presents the key result of our work. It shows the luminosity of the BLR as a function of the observed γ-ray luminosity, both measured in Eddington units. The arrows correspond to the upper limits. Different symbols correspond to blazars belonging to different samples, as labelled. Note that we have also added the blazars studied in G11, but we have omitted the objects in common. Fig. 2 shows a clear trend. Because the range of black hole masses is relatively narrow, we obtain a similar trend when plotting $L_{\rm BLR}$ versus L_γ. We have quantified this first by using the Kendall non-parametric test, considering the detected sources (i.e. excluding upper limits). The Kendall τ in this case is listed in Table 5.

Table 4. Blazars from G11. The columns give the following: (1) name; (2) right ascension; (3) declination; (4) redshift; (5) logarithm of the black hole mass (in solar masses); (6) BLR luminosity (10^{42} erg s^{-1}); (7) γ-ray luminosity (10^{45} erg s^{-1}). 'FS' stands for flat spectrum quasars, following the classification in G11.

Name	RA	Dec.	z	$\log M\,\mathrm{M}_{\odot}^{-1}$	$L_{\rm BLR}$ (10^{42} erg s^{-1})	L_{γ} (10^{45} erg s^{-1})
(1)	(2)	(3)	(4)	(5)	(6)	(7)
'FS'						
PKS 0208−512	02 11 13.18	+10 51 34.8	1.003	9.2	3700	489.8
PKS 0235+164	02 38 38.93	+16 36 59.3	0.940	9.0	100	1737.8
PKS 0426−380	04 28 40.42	−37 56 19.6	1.111	8.6	110	1513.6
PKS 0537−441	05 38 50.35	−44 05 08.7	0.892	8.8	690	1000.0
PKS 0808+019	08 11 26.71	+01 46 52.2	1.148	8.5	42	120.2
LBL						
PKS 0521−36	05 22 57.98	−36 27 30.9	0.055	8.6	4.8	0.28
PKS 0829+046	08 31 48.88	+04 29 39.1	0.174	8.8	3.7	2.45
OJ 287	08 54 48.87	+20 06 30.6	0.306	8.8	6.8	1.51
TXS 0954+658	09 58 47.25	+65 33 54.8	0.367	8.5	2.8	4.90
PMN 1012+0630	10 12 13.35	+06 30 57.2	0.727	8.5	7.8	35.5
PKS 1057−79	10 58 43.40	−80 03 54.2	0.581	8.8	58	45.7
PKS 1519−273	15 22 37.68	−27 30 10.8	1.294	8.8	34	354.8
PKS 1749+096	17 51 32.82	+09 39 00.7	0.322	8.7	50	26.9
S5 1803+78	18 00 45.68	+78 28 04.0	0.680	8.6	710	87.1
3C 371	18 06 50.68	+69 49 28.1	0.050	8.7	1.0	0.19
BL Lac	22 02 43.29	+42 16 40.0	0.069	8.7	3.3	0.93
PKS 2240−260	22 43 26.47	−25 44 31.4	0.774	8.6	29	56.23
HBL						
Mkn 421	11 04 27.30	+38 12 32.0	0.031	8.5	0.5	0.33
Mkn 501	16 53 52.20	+39 45 37.0	0.034	9.0	1.6	0.09
PKS 2005−489	20 09 25.40	−48 49 54.0	0.071	8.5	1.1	0.32
WGA 1204.2−0710	12 04 16.66	−07 10 09.0	0.185	8.8	<9.5	0.98
FSRQ						
TXS 1013+054	10 16 03.10	+05 13 02.0	1.713	9.5	889	1584.9
S4 1030+61	10 33 51.40	+60 51 07.3	1.401	9.5	450	741.31
PKS 1144−379	11 47 01.40	−38 12 11.0	1.049	8.5	400	223.9
3C 273	12 29 06.69	+02 03 08.5	0.158	8.9	3380	21.4
3C 279	12 56 11.10	−05 47 21.5	0.536	8.9	242	204.2
PKS 1510−089	15 12 50.50	−09 06 00.0	0.360	8.6	741	125.9
OX 169	21 43 35.50	+17 43 48.6	0.213	8.6	182	8.51
CTA102	22 32 36.40	+11 43 53.8	1.037	8.7	4140	489.8
3C 454.3	22 53 57.70	+16 08 53.6	0.859	8.7	3330	5011.9

The correlation is significant, both when considering $\log L_{\rm BLR}$ versus $\log L_{\gamma}$ and when measuring these quantities in Eddington units. Thus, we have considered the common dependence upon the redshifts of both luminosities, and we have applied the partial Kendall correlation analysis, as described in Akritas & Siebert (1996). The correlation is still significant, although with a smaller τ. We have then included the upper limits, and by repeating the same analysis, we have verified that the value of τ is now greater.

Finally, we applied a simple least-squares fit and performed a partial correlation analysis (see equation 1 of Padovani 1992), taking into account the common dependence on the redshift and on the black hole mass of the plotted quantities. The results are listed in Table 6. In this case, we have excluded all upper limits from the analysis.

Before discussing the implications of this correlation, there are a few caveats to note, concerning possible important selection effects.

(i) In the 1LAC catalogue, there are many detected sources without a known redshift. As discussed in Abdo et al. (2010b) and G11, if these sources were found to be at $z \sim 2$, then their γ-ray luminosities would be huge. If the absence of broad emission lines is a result of their intrinsic weakness, then these blazars would be located in the bottom-right part of Fig. 2, and they would be clear outliers of the found correlation. If, instead, the absence of lines is the result of a particularly strong non-thermal continuum, then $L_{\rm BLR}$ could be large, which would locate these objects in the 'FSRQs quadrant'.

(ii) We have clear examples of blazars whose γ-ray luminosities vary by more than two orders of magnitude. It is very likely that the present samples of γ-ray-detected blazars preferentially include objects in their high state.[1] The γ-ray luminosity we have considered is the average over 11 months (therefore, the short term variability is averaged for), but blazars can be variable over longer periods. This variability introduces an inevitable dispersion around the correlation line.

(iii) Misaligned jets should be weaker γ-ray sources than their aligned counterparts, but they would show the same emission-line luminosities. Therefore, weak γ-ray sources must exist, which

[1] This would also explain why the radio and γ-ray fluxes are correlated, even if only a relatively small fraction of radio-loud AGNs with a flat spectrum are detected in γ-rays (e.g. Ghirlanda et al. 2011).

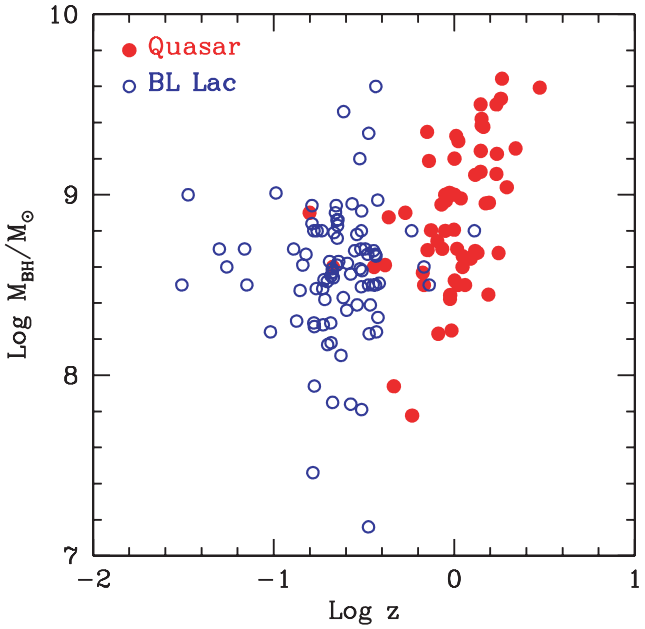

Figure 1. Black hole masses as a function of redshift. Empty circles are BL Lacs and filled circles are FSRQs. The BL Lacs of our sample have significantly smaller redshifts than the FSRQs.

would populate the region to the left of the interpolating line of Fig. 2. However, these sources would be classified as radio galaxies (see Abdo et al. 2010c) and not aligned blazars, although some overlap might exist.

Despite the above caveats, the apparent correlation between the BLR and the jet γ-ray luminosity is certainly intriguing, because it would prove the importance of the emission-line photons in the production of high-energy γ-rays. More importantly, it would point towards a relation between the accretion rate and the jet power. This relation is not direct, however, because the observed γ-ray luminosity can be considered a poor proxy of the jet power, and the disc luminosity is linearly related to the accretion rate only for a 'standard' optically thick geometrically thin accretion disc. This is discussed further in Section 5.

Fig. 2 shows that BL Lacs are neatly divided from FSRQs: with a few exceptions, all FSRQs have $L_{\rm BLR}/L_{\rm Edd} > 5 \times 10^{-4}$ and all BL Lacs are below this value. The corresponding dividing γ-ray luminosity is $L_{\gamma}/L_{\rm Edd} \sim 0.1$. We have derived this apparent 'divide' by considering only the sources for which we have a detection of the BLR and the γ-ray luminosities. In other words, we first excluded the upper limits from the analysis. The lack of data does not allow us to reach a firm conclusion about the exact value of this divide. However, reassuringly, when we include all the upper limits, they lie in the 'correct' quadrant of the plane.

However, most upper limits correspond to BL Lacs with $z < 0.4$, so an issue remains: the divide between BL Lacs and FSRQs could be partly a result of the segregation in redshift, if all BL Lacs are at low redshift and FSRQs at high redshift. To verify this, in Fig. 3 we plot the BLR luminosity (in Eddington units) as a function of redshift. It can be seen that there are detected BL Lacs with $L_{\rm BLR}/L_{\rm Edd} < 5 \times 10^{-4}$ at relatively large redshifts. This is a hint that the divide is real, but, again, the lack of points precludes a more definite conclusion about this possible selection effect. Moreover, most of the upper limits come from the P11 sample, which by construction selects only BL Lacs at $z < 0.4$. This limit in redshift possibly introduces a bias in the dividing value, as can be seen in Fig. 3. Nevertheless, we reiterate that the upper limits were not used in the determination of the divide, and hence this bias does not completely compromise the result.

If real, the divide found would be in agreement with that found when studying the distribution of bright *Fermi*-detected blazars in the γ-ray spectral index–γ-ray luminosity plane (for them Ghisellini et al. 2009, proposed a "divide" between BL Lacs and FSRQs around $L_{\rm d}/L_{\rm Edd} \sim 10^{-2}$), and with that more recently found by G11 when using a sample of bright blazars much more limited in number than we have used here. The value of the divide found here would also be consistent with the division between FR I and FR II radio galaxies, which was found by Ghisellini & Celotti (2001) using a completely different approach.

Fig. 2 also shows that all blazars form a continuous family, with no apparent 'discontinuity' (or sign of bimodality). Excluding the upper limits, we have found that $L_{\rm BLR} \propto L_{\gamma}$ (normalizing or not to Eddington). Then, the question is whether it is still meaningful to divide BL Lacs from FSRQs, because in Fig. 2 they form a continuous distribution. In other words, are BL Lacs and FSRQs characterized by some different fundamental properties, or are they simply on two sides of a continuous distribution of properties? An example can illustrate this point. Suppose, as suggested by Ghisellini et al. (2009), that the accretion discs in BL Lacs are radiatively inefficient, while they are efficient in FSRQs. This is a fundamentally different property, although it concerns the accretion disc, not the jet. Another example is to suppose that jets in BL Lacs are made by pure electron–positron plasmas, while the jets in FSRQs are made by normal electron–proton plasmas. This, too, should be considered a fundamentally different property. If, instead, all blazars have radiatively efficient accretion discs and their jets are all made by electrons and protons, then they look different only because they have different overall powers. This, in turn, might also explain why their spectral energy distributions (SEDs) are different, without the need for anything fundamental to divide them.

The following discussion concerns this issue, focusing in particular on the proposed 'divide' between BL Lacs and FSRQs in terms of the mass accretion rate in Eddington units.

5 DISCUSSION

Our study concerns $L_{\rm BLR}$, L_{γ}, and the black hole mass. In the following, we discuss how we can use $L_{\rm BLR}$ to find the disc luminosity $L_{\rm d}$, and how we can use L_{γ} to find a proxy for the jet power $P_{\rm jet}$ and the mass accretion rate $\dot{M}$. The black hole mass is, of course, used to normalize all powers to the Eddington luminosity.

$L_{\rm BLR} \rightarrow L_{\rm d} \rightarrow \dot{M}$

For radiatively efficient accretion discs, the BLR luminosity is a direct measure of the disc luminosity $L_{\rm d}$, because, on average, $L_{\rm d} \sim 10\,L_{\rm BLR}$ (e.g. Baldwin & Netzer 1978; Smith et al. 1981). A radiatively efficient disc (e.g. Shakura & Sunyaev 1973) should occur for $\dot{m} \equiv \dot{M}/\dot{M}_{\rm Edd} > \dot{m}_{\rm c}$. Defining $\dot{M}_{\rm Edd} \equiv L_{\rm Edd}/c^2$ (without the efficiency factor), then $\dot{m}_{\rm c}$ should be close to 0.1 (Narayan & Yi 1995). Another hypothesis suggests the lower value $\dot{m}_{\rm c} \sim 10^{-4}$ for the radiative transition (Sharma et al. 2007). If the disc emits as a blackbody at all radii, then most of the power is emitted in the far-ultraviolet, and we can approximate the photoionizing luminosity with the entire $L_{\rm d}$.

When $\dot{m} < \dot{m}_{\rm c}$, the disc should become radiatively inefficient, because the particle density of the accretion flow becomes small,

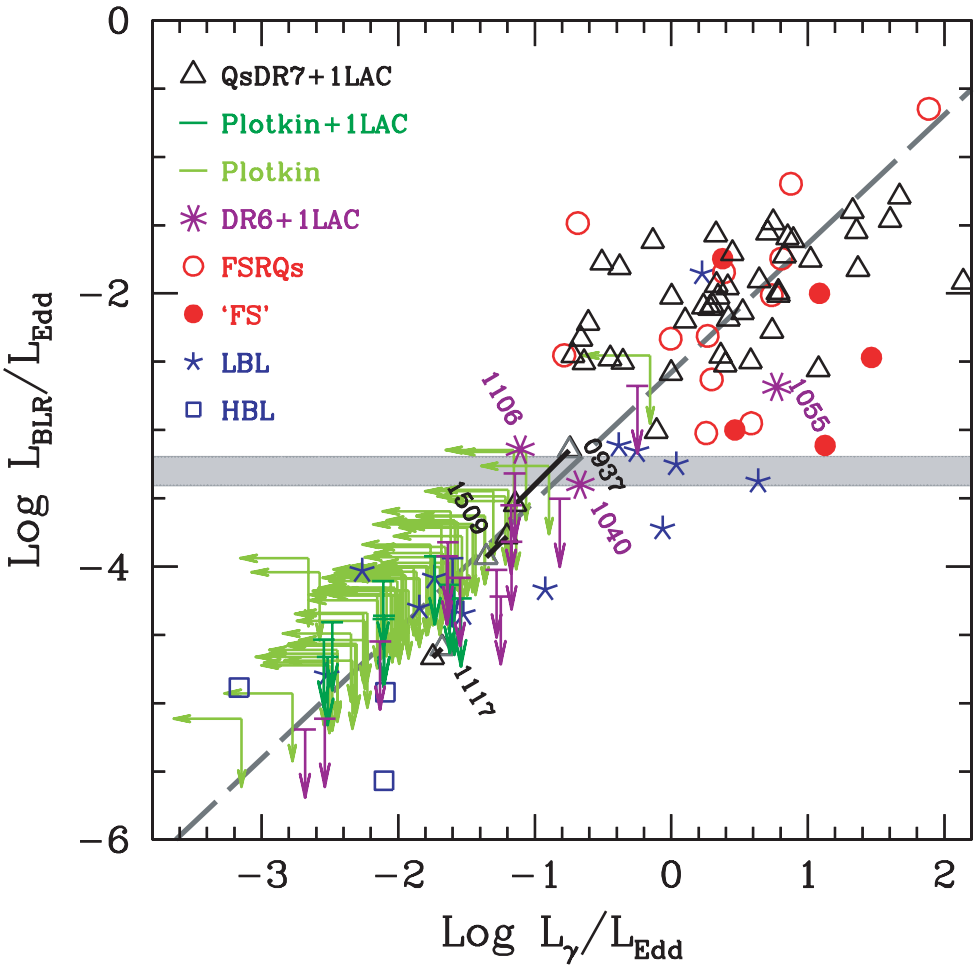

Figure 2. Luminosity of the BLR (in Eddington units) for the sources from our samples and from G11 as a function of the γ-ray luminosity (in Eddington units). Different symbols correspond to different samples or a different classification of the sources, as labelled. The three (violet) asterisks are the only sources with visible broad emission lines from the SDSS DR6 *Fermi*-detected sample. The three labelled triangles have their synchrotron emission dominating over the thermal emission in their SEDs. Hence, to avoid errors in the estimates of the black hole mass, which possibly occur in the S11 automatic calculation, we have also assigned them an average $M_{\rm BH}$ value ($M_{\rm BH} = 5 \times 10^8$ M$_\odot$). These changes are highlighted by the thick (black) segments ending at the black triangles (corresponding to the average $M_{\rm BH}$ value). The grey stripe indicates the luminosity 'divide' between FSRQs and BL Lacs at $L_{\rm BLR}/L_{\rm Edd} \sim 5 \times 10^{-4}$.

Table 5. The results of the non-parametric Kendall test for the complete sample, first taking into consideration only the sources with both $L_{\rm BLR}$ and L_γ detected, then including the upper limits. We also list the results when accounting for the common dependence on redshift.

Kendall test	τ	
	Det.	Det. + UL
$\log L_{\rm BLR}$–$\log L_\gamma$	0.530	0.561
$\log L_{\rm BLR}$–$\log L_\gamma$, z	0.281	0.386
$\log(L_{\rm BLR}/L_{\rm Edd})$–$\log(L_\gamma/L_{\rm Edd})$	0.398	0.529
$\log(L_{\rm BLR}/L_{\rm Edd})$–$\log(L_\gamma/L_{\rm Edd})$, z	0.266	0.376

and the energy exchange time-scale between protons and electrons becomes smaller than the accretion time. If this occurs, the disc bolometric luminosity decreases. Narayan et al. (1997) proposed that, in this regime, $L_{\rm d} \propto \dot{M}^2$. In this case, the disc becomes hot, inflates, and it does not emit blackbody radiation. As a consequence, $L_{\rm ion} \ll L_{\rm d}$. According to Mahadevan (1997) – see his fig. 1– the decreasing fraction of the ionizing luminosity is as important as the decrease of the overall efficiency η (defined as $L_{\rm d} = \eta \dot{M} c^2$). In the example shown by fig. 1 of Mahadevan (1997), $L_{\rm ion} \propto \dot{M}^{3.5}$. If this were true, we would also expect the broad emission-line luminosity to have the same dependence on $\dot{M}$ when $\dot{M}$ goes subcritical. Note, however, that the SED calculated by Mahadevan (1997) could be greatly affected by the presence of extra sources of seed photons for the thermal Componization, besides the assumed cyclotron–synchrotron emission. These extra seed photons (for instance, coming from some cool part of the disc) could enhance the ultraviolet emission, both by enhancing the Compton scattering and by cooling the hot emitting electrons. So, we regard the $L_{\rm BLR} \propto L_{\rm ion} \propto \dot{M}^{3.5}$ relation as an indication, but without excluding other possibilities. In practice, for $\dot{m} < \dot{m}_{\rm c}$, we consider both $L_{\rm BLR} \propto \dot{M}^2$ and $L_{\rm BLR} \propto \dot{M}^{3.5}$.

$L_\gamma \rightarrow P_{\rm jet} \rightarrow \dot{M}$

A lower limit on the jet power $P_{\rm jet}$ is

$$P_{\rm jet} > P_{\rm r} \gtrsim \frac{L_{\rm bol}}{\Gamma^2}, \quad (1)$$

where Γ is the bulk Lorentz factor (see Celotti & Ghisellini 2008; Ghisellini & Tavecchio 2009), $L_{\rm bol}$ is the jet bolometric luminosity,

Table 6. The results of a partial correlation analysis using a least-squares fit. We have excluded the upper limits from the analysis. The correlations are of the form $\log y = m \log x + q$. The listed slopes m refer to the bisector (of the two correlations x versus y and y versus x). N is the total number of objects, r is the correlation coefficient obtained from the analysis and P is the probability that the correlation is random.

Minimum square fit (detections only)	m	q	N	r	P
$\log L_{\rm BLR}$–$\log L_\gamma$	0.93	0.61	78	0.83	$<4 \times 10^{-8}$
$\log L_{\rm BLR}$–$\log L_\gamma$, z	0.93	0.61	78	0.64	$<4 \times 10^{-8}$
$\log(L_{\rm BLR}/L_{\rm Edd})$–$\log(L_\gamma/L_{\rm Edd})$	0.94	−2.58	78	0.78	$<4 \times 10^{-8}$
$\log(L_{\rm BLR}/L_{\rm Edd})$–$\log(L_\gamma/L_{\rm Edd})$, z	0.94	−2.58	78	0.67	$<4 \times 10^{-8}$
$\log(L_{\rm BLR}/L_{\rm Edd})$–$\log(L_\gamma/L_{\rm Edd})$, z, M	0.94	−2.58	78	0.64	$<4 \times 10^{-8}$

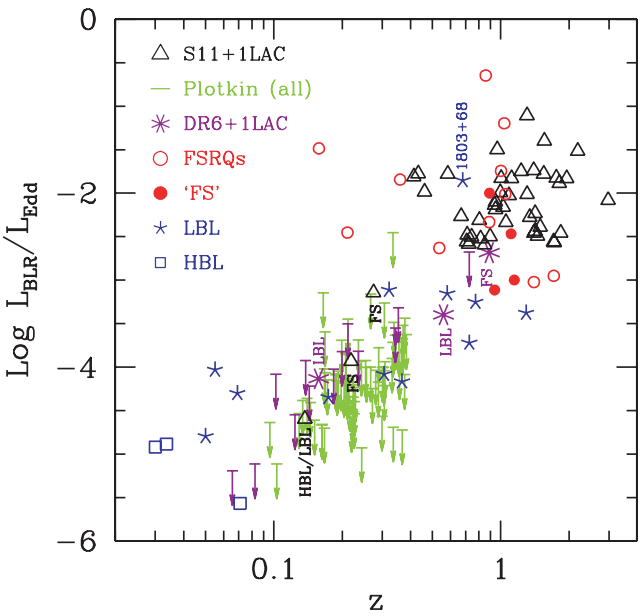

Figure 3. The broad line luminosity (in Eddington units) as a function of redshift. The symbols are the same as in Fig. 2.

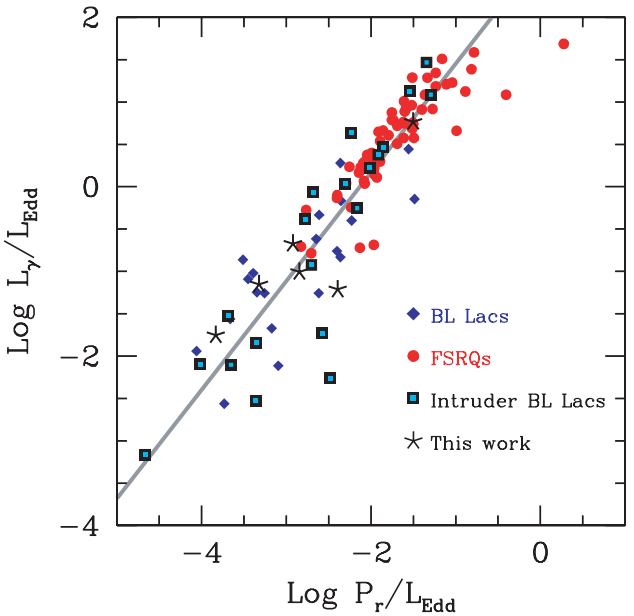

Figure 4. The γ-ray luminosity in the LAT band as a function of the jet power $P_{\rm r}$ (both in Eddington units). The latter is the power that the jet has spent to produce the (bolometric) radiation we see; this is given by $P_{\rm r} \sim L_{\rm bol}/\Gamma^2$. To derive this, we have used blazars detected by *Fermi*, for which we have constructed the SED and estimated the bulk Lorentz factor (G10; G11; Tavecchio et al. 2010). The grey solid line shows the result (bisector) of a least-squares fit.

measured assuming isotropic emission, and $P_{\rm r}$ is the power that the jet has to spend to produce the radiation we see. If $P_{\rm jet} \sim P_{\rm r}$, then the jet uses its entire power to produce radiation, including its kinetic power, and it should stop. By fitting the SEDs of a large number of blazars detected by *Fermi* with a simple one-zone leptonic model (such as the one used in Appendix A) we obtain values of Γ contained in a narrow range, around 13–15 (see Ghisellini et al. 2010, hereafter G10), consistent with the values derived from the superluminal motion. The same model also yields the number of emitting electrons required to account for the radiation we see. By assuming one proton per electron, we obtain $P_{\rm jet} \sim 30$–$100\,P_{\rm r}$, on average. We can conclude that $P_{\rm jet}$ is robustly bound to be larger than $P_{\rm r} \sim L_{\rm bol}/200$, and it can be a factor 30–100 larger than that.

The key result obtained in G10 (confirming earlier results in Celotti & Ghisellini 2008, and then also confirmed by G11) is that $P_{\rm jet} \sim \dot{M}c^2$. Because $P_{\rm r}$ is linearly related to $P_{\rm jet}$, and it is a model-independent quantity, we can safely use $P_{\rm r}$ as a proxy for $P_{\rm jet}$ and $\dot{M}$. To measure $P_{\rm r} \sim L_{\rm bol}/\Gamma^2$, we should construct the SED of all our blazars. However, we can take advantage of the sample already studied in the literature, to find out if there is a robust relation between $P_{\rm r}$ and the γ-ray luminosity L_γ in the *Fermi*/LAT energy range, which is the quantity most readily available to us. Such a robust relation does exist, and it is shown in Fig. 4. By fitting this with a simple least-squares method and by taking the bisector, we obtain

$$\mathrm{Log}\left(\frac{L_\gamma}{L_{\rm Edd}}\right) = 1.284\ \mathrm{Log}\left(\frac{P_{\rm r}}{L_{\rm Edd}}\right) + 2.738. \quad (2)$$

Note that the two quantities are not linearly related. At low values of $L_\gamma/L_{\rm Edd}$, the γ-ray luminosity underestimates $P_{\rm r}$ (either normalizing or not to the Eddington luminosity). As a consequence, the $L_\gamma/L_{\rm Edd}$ values for low-luminosity BL Lacs underestimate the jet power, and in turn the mass accretion rate. This occurs because L_γ is not a good indicator of $L_{\rm bol}$ for low-luminosity BL Lacs, which have their high-energy SEDs peaking in the TeV band and also have an important (often dominant) synchrotron component.

$L_{\rm BLR}/L_{\rm Edd}$ versus $P_{\rm r}/L_{\rm Edd}$

Because the above correlation appears to be robust, we can use it to obtain $P_{\rm r}/L_{\rm Edd}$ from our values of L_γ and black hole mass, without the need to construct the SED and to model it. In turn, we can think of the obtained $P_{\rm r}/L_{\rm Edd}$ values as proportional to the mass

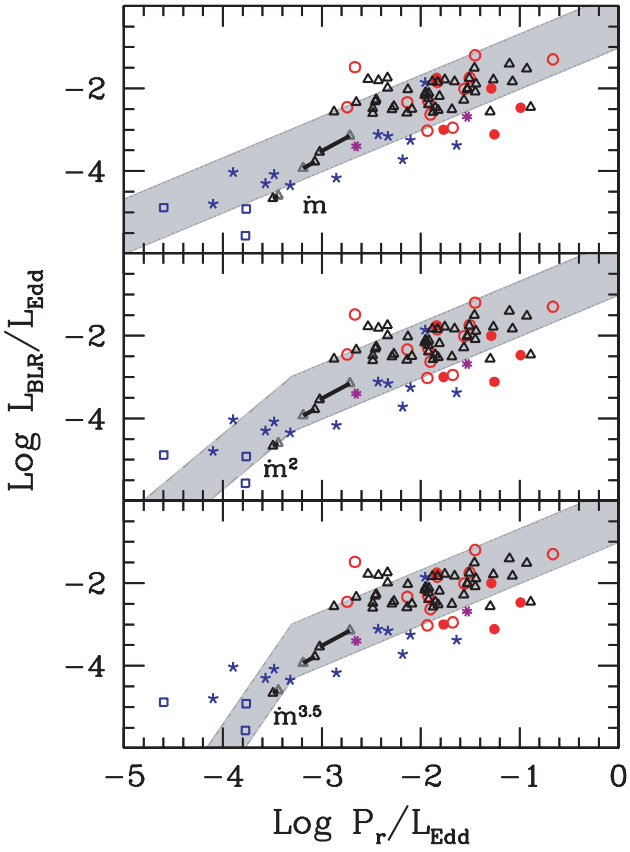

Figure 5. Luminosity of the BLR (in Eddington units) for the sources from our samples and from G11 as a function of P_r (in Eddington units). The symbols are the same as in Fig. 2, but without upper limits and with grey stripes superimposed. In all three panels, we assume that P_r tracks $\dot{M}$. If this is true, we can see how the broad line luminosity is related to $\dot{m} \equiv \dot{M}/\dot{M}_{Edd}$ or, equivalently, to P_r/L_{Edd}. At large values of L_{BLR}/L_{Edd}, the grey stripe in all panels corresponds to $L_{BLR}/L_{Edd} \propto P_r/L_{Edd}$. In the top panel, the grey stripe continues to show a linear relation also at low values of L_{BLR}/L_{Edd}. In the middle panel, the grey stripe becomes quadratic below some critical value (here $L_\gamma/L_{Edd} = 0.1$ is assumed, i.e. the value dividing BL Lacs from FSRQs). In the bottom panel, the grey stripe becomes $L_{BLR}/L_{Edd} \propto (P_r/L_{Edd})^{3.5}$ at low values, to account for the deficit of ionizing ultraviolet photons in a radiatively inefficient disc.

accretion rate in Eddington units. This is done in Fig. 5 where we plot L_{BLR}/L_{Edd} as a function of P_r/L_{Edd}.

For $\dot{m} > \dot{m}_c$, we expect the BLR luminosity, in Eddington units, to depend linearly on the normalized accretion rate, and therefore $L_{BLR}/L_{Edd} \propto \dot{m} \propto P_r/L_{Edd}$.

Below $\dot{m} \sim \dot{m}_c$, we expect the disc to become radiatively inefficient. The disc's bolometric luminosity becomes proportional to $\dot{m}^2$, while the ionizing luminosity can follow an even steeper relation with $\dot{m}$ (i.e. $\propto \dot{m}^{3.5}$; see above). In Fig. 5, the grey stripe at small L_{BLR}/L_{Edd} is proportional to P_r/L_{Edd} in the top panel, to $(P_r/L_{Edd})^2$ in the mid panel and to $(P_r/L_{Edd})^{3.5}$ in the bottom panel. We mainly consider the hypothesis of $m_c \sim 0.1$ proposed by Narayan & Yi (1995). The break value has been chosen to correspond to $L_{BLR}/L_{Edd} \sim 5 \times 10^{-4}$, allowing for considerable scatter around this value. Note that, if we take into account the $m_c \sim 10^{-4}$ hypothesis (Sharma et al. 2007), the break values would be outside the luminosity range of our sample.

Fig. 5 shows that we cannot yet distinguish among the different cases, even if there is some preference for the $L_{BLR}/L_{Edd} \propto (P_r/L_{Edd})^2$ case.

There are HBL-type BL Lacs, such as Mkn 421, Mkn 501 and 2005–489, that do show broad emission lines (and prototypical BL Lacs too, i.e. a BL Lac itself), with L_{BLR} around 10^{42} erg s^{-1} and L_{BLR}/L_{Edd} around 10^{-5}. These are the objects at the low (bottom-left) end of Figs 2, 4 and 5. We need more low-power BL Lacs to investigate if they are indeed associated with radiatively inefficient discs.

Note that this is not necessary for the basic explanation of the blazar sequence and for the proposed luminosity 'divide' between BL Lacs and FSRQs. In fact, the change of the observed SED along the blazar sequence, interpreted as a radiatively cooling sequence (Ghisellini et al. 1998), requires that in BL Lacs the emission lines are not as important as seed photons for the inverse Compton process. This can be the case even if the lines are present, if the dissipation region occurs outside R_{BLR}; in this case, the BLR photons are seen in the comoving region, redshifted and time-diluted, and the external compton (EC) process can be negligible. The relation between the size of the BLR and the ionizing luminosity ensures that in BL Lacs the size of the BLR is much smaller than in FSRQs, even if the black hole mass is similar. If dissipation always occurs at $R_{diss} \sim 10^3$ Schwarzschild radii, then for BL Lacs we easily have $R_{diss} > R_{BLR}$ (and emitting lines are negligible for the formation of the high-energy spectrum), while for the more powerful FSRQs we have $R_{diss} < R_{BLR}$, with a corresponding enhancement of the EC process. In earlier works (Celotti & Ghisellini 2008; G10; G11), it has been shown that R_{diss} is of the order of $\sim 10^3$ Schwarzschild radii in all objects. Requiring that the size of the BLR is a factor f smaller than this, and using $R_{BLR} = 10^{17} L_{d,45}^{1/2}$ cm, we obtain

$$R_{BLR} < f R_{diss} \rightarrow \frac{L_d}{L_{Edd}} < 6.9 \times 10^{-3} f^2 M_8 \left(\frac{R_{diss}}{10^3\, R_S} \right)^2, \quad (3)$$

where $M = 10^8 M_8$ solar masses. We obtain, in this case, a value for the divide that agrees with the observed $L_{BLR}/L_{Edd} \sim 5 \times 10^{-4}$ (for $L_{BLR} \sim 0.1 L_d$ and f smaller than, but close to, unity), but dependent on the black hole mass. The dependence on the black hole mass would produce some blur in the division, which is not inconsistent with what we see.

6 CONCLUSIONS

In this work, we have studied the blazars that have been detected by *Fermi*/LAT and that are present in the SDSS optical survey, for which the redshift is known and for which there is an estimate of the black hole mass. From the broad emission-line luminosities (or their upper limits), we have calculated the luminosity of the entire BLR, used as a proxy for the luminosity of the accretion disc. We were able to find values for both the BLR and the γ-ray luminosity for 78 blazars, values for L_{BLR} and the upper limits on L_γ for 23 blazars and the upper limits on both quantities for 62 sources. Our results can be summarized as follows.

(i) The luminosity of the BLR correlates well with the γ-ray luminosity in the *Fermi*/LAT energy range. The correlation is linear, irrespective of whether the above luminosities are normalized to the Eddington value or not. All upper limits (not used to find the correlation) are consistent with the correlation itself.

(ii) BL Lacs and FSRQs occupy different regions of the L_{BLR}/L_{Edd}–L_γ/L_{Edd} plane, with a division at about $L_{BLR}/L_{Edd} \sim 5 \times 10^{-4}$. Using an enlarged sample, this confirms earlier results.

Nevertheless, because the sample still lacks sources with detections on both $L_{\rm BLR}$ and L_γ and is instead rich in upper limits, this 'divide' still needs to be studied further using a more populated sample.

(iii) For objects (analysed in previous works) of known L_γ, $P_{\rm r}$, and black hole mass, there is a strong correlation between the two quantities, both using absolute values and normalizing them to the Eddington luminosity: $(L_\gamma/L_{\rm Edd}) \propto (P_{\rm r}/L_{\rm Edd})^{1.28}$. As a consequence, the γ-ray luminosity (in the *Fermi*/LAT energy range) can be used to estimate $P_{\rm r}$, which is a robust proxy for the jet power.

(iv) The relation between the strength of the emission lines and the accretion rate can be used to test radiatively inefficient disc models and the prediction about the production, in these discs, of the ionizing luminosity. Our results are too primitive to draw strong conclusions, but there is the possibility that, at low accretion rates, the produced ionizing ultraviolet luminosity is larger than expected.

(v) The division between BL Lacs and FSRQs could be a result of the transition between a radiatively inefficient disc to a standard (Shakura–Sunyaev) disc. Alternatively, it could be a result of the dissipation region of the jet being located outside or inside the BLR.

ACKNOWLEDGMENTS

We thank the referee for useful comments that have improved the paper. We thank Julian Krolik for suggesting the possibility of a transition to the advection-dominated accretion flow at accretion rates smaller than those we have considered. We also thank F. Tavecchio, G. Ghirlanda and L. Foschini for discussions. In this research, we made use of the NASA/IPAC Extragalactic Data base (NED), which is operated by the Jet Propulsion Laboratory, Caltech, under contract with NASA, and we also used the *Swift* public data, made available by the HEASARC archive system.

REFERENCES

Abdo A. A. et al., 2009, ApJ, 700, 597
Abdo A. A. et al., 2010a, ApJ, 715, 429
Abdo A. A. et al., 2010b, ApJ, 716, 30
Abdo A. A. et al., 2010c, ApJ, 720, 912
Ackermann M. et al., 2012, ApJ, 743, 171
Adelman-McCarthy J. K. et al., 2008, ApJS, 175, 297
Akritas M. G., Siebert J., 1996, MNRAS, 278, 919
Baldwin J. A., Netzer H., 1978, ApJ, 226, 1
Celotti A., Ghisellini G., 2008, MNRAS, 385, 283
Celotti A., Padovani P., Ghisellini G., 1997, MNRAS, 286, 415
Chiaberge M., Marconi A., 2011, MNRAS, 416, 917
Condon J. J., Cotton W. D., Greisen E. W., Yin Q. F., Perley R. A., Taylor G. B., Broderick J. J., 1998, AJ, 115, 1693
Decarli R., Dotti M., Treves A., 2011, MNRAS, 413, 39
D'Elia V., Padovani P., Landt H., 2003, MNRAS, 339, 1081
Francis P. J., Hewett P. C., Foltz C. B., Chaffee F. H., Weymann R. J., Morris S. L., 1991, ApJ, 373, 465
Ghirlanda G., Ghisellini G., Tavecchio F., Foschini L., Bonnoli G., 2011, MNRAS, 413, 852
Ghisellini G., Celotti A., 2001, A&A, 379, L1
Ghisellini G., Tavecchio F., 2009, MNRAS, 397, 985
Ghisellini G., Celotti A., Fossati G., Maraschi L., Comastri A., 1998, MNRAS, 301, 451
Ghisellini G., Maraschi L., Tavecchio F., 2009, MNRAS, 396, L105
Ghisellini G., Tavecchio F., Foschini L., Ghirlanda G., Maraschi L., Celotti A., 2010, MNRAS, 402, 497 (G10)
Ghisellini G., Tavecchio F., Foschini L, Ghirlanda G., 2011, MNRAS, 414, 2674 (G11)
Landt H., Padovani P., Giommi P., 2002, MNRAS, 336, 945
Landt H., Padovani P., Giommi P., Perlman E. S., 2004, MNRAS, 351, 83
León-Tavares J., Valtaoja E., Chavushyan V. H., Tornikoski M., Añorve C., Nieppola E., Lähteenmäki A., 2011, MNRAS, 411, 1127
Mahadevan R., 1997, ApJ, 447, 585
Marcha M. J. M., Browne I. W. A., Impey C. D., Smith P. S., 1996, MNRAS, 281, 425
Mattox J. R. et al., 1996, ApJ, 461, 396
Narayan R., Yi I., 1995, ApJ, 452, 710
Narayan R., Garcia M. R., McClintock J. E., 1997, ApJ, 478, L79
Padovani P., 1992, A&A, 256, 399
Padovani P., Giommi P., 1995, ApJ, 444, 567
Plotkin R. M., Anderson S. F., Hall P. B., Margon B., Voges W., Schneider D. P., Stinson G., York D. G., 2008, AJ, 135, 2453
Plotkin R. M. et al., 2010, AJ, 139, 390
Plotkin R. M., Markoff S., Trager S. C., Anderson S. F., 2011, MNRAS, 413, 805 (P11)
Scarpa R., Falomo R., 1997, A&A, 325, 109
Shakura N. I., Sunyaev R. A., 1973, A&A, 24, 337
Sharma P., Quataert E., Hammet G. H., Stone J. M., 2007, ApJ, 667, 714
Shen Y. et al., 2011, ApJS, 194, 45 (S11)
Smith M. G. et al., 1981, MNRAS, 195, 437
Tavecchio F., Ghisellini G., Ghirlanda G., Foschini L., Maraschi L., 2010, MNRAS, 401, 1570
Urry C. M., Padovani P., 1995, PASP, 107, 803
White R. L., Becker R. H., Helfand D. J., Gregg M. D., 1997, ApJ, 475, 479
York D. G. et al., 2000, AJ, 120, 1579

APPENDIX A:

A1 Spectral energy distribution

We have characterized the SEDs of the six sources for which we have both the spectroscopic optical data and the detection by *Fermi*. We have collected the data from the NED and we have included the LBAS and 1LAC *Fermi*/LAT data (Abdo et al. 2010a,b).

A2 Model

To model the SEDs, we have used the leptonic, one-zone synchrotron and inverse Compton models, which are fully discussed in Ghisellini & Tavecchio (2009).

In brief, we assume that in a spherical region of radius R, located at a distance $R_{\rm diss}$ from the central black hole, relativistic electrons are injected at a rate $Q(\gamma)$ (cm^{-3} s^{-1}) for a finite time equal to the light crossing time R/c. For the shape of $Q(\gamma)$, we adopt a smoothly broken power law, with a break at $\gamma_{\rm b}$:

$$Q(\gamma) = Q_0 \frac{(\gamma/\gamma_{\rm b})^{-s_1}}{1+(\gamma/\gamma_{\rm b})^{-s_1+s_2}}. \quad \text{(A1)}$$

The emitting region is moving with a velocity βc, corresponding to a bulk Lorentz factor Γ. We observe the source at the viewing angle $\theta_{\rm v}$ and the Doppler factor is $\delta = 1/[\Gamma(1-\beta\cos\theta_{\rm v})]$. The magnetic field B is tangled and uniform throughout the emitting region. We take into account several sources of radiation externally to the jet: (i) the broad-line photons, assumed to re-emit 10 per cent of the accretion luminosity from a shell-like distribution of clouds located at a distance $R_{\rm BLR} = 10^{17} L_{\rm d,45}^{1/2}$ cm; (ii) the infrared emission from a dusty torus, located at a distance $R_{\rm IR} = 2.5 \times 10^{18} L_{\rm d,45}^{1/2}$ cm; (iii) the direct emission from the accretion disc, including its X-ray corona; (iv) the starlight contribution from the inner region of the host galaxy; (v) the cosmic background radiation. All these contributions are evaluated in the blob comoving frame, where we calculate the corresponding inverse Compton radiation from all

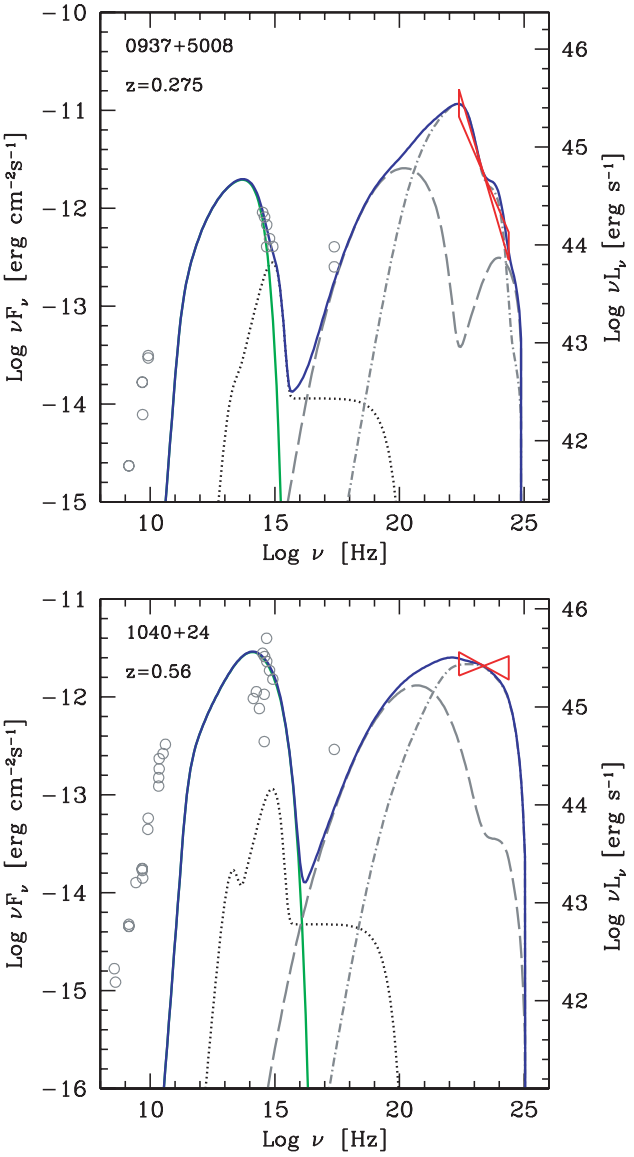

Figure A1. SEDs of 0937+5508 and 1040+24 and the fitting model. The dotted line corresponds to emission from the accretion disc, the infrared torus (if present) and the X–ray corona. The thin (green) solid line is the synchrotron component, the long-dashed line is the synchrotron self-Compton (SSC) emission and the dot-dashed line is the EC contribution. The thick (blue) solid line is the sum.

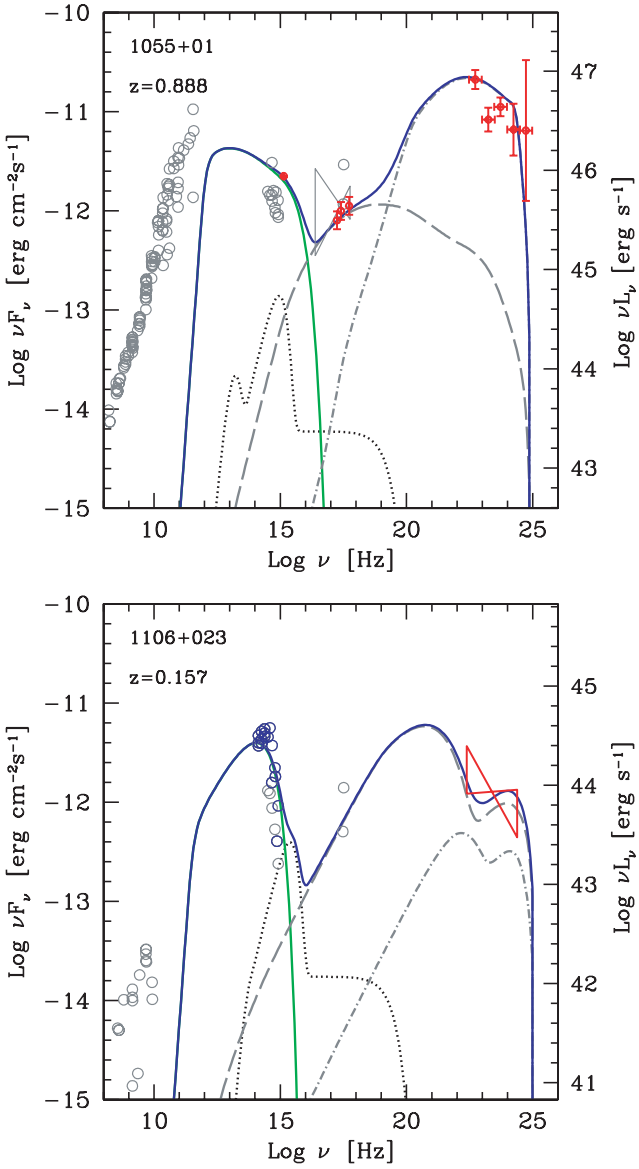

Figure A2. SEDs of 1055+01 and 1106+023. The lines are the same as in Fig. A1.

these contributions, and then transformed into the observer frame. The latter two contributions are negligible for our sources.

We calculate the energy distribution $N(\gamma)$ (cm^{-3}) of the emitting particles at the particular time R/c, when the injection process ends. Our numerical code solves the continuity equation, which includes injection, radiative cooling and e$^{\pm}$ pair production and reprocessing. Our code is not a time-dependent code: we give a 'snapshot' of the predicted SED at the time R/c, when the particle distribution $N(\gamma)$ and, consequently, the produced flux are at their maximum.

To calculate the flux produced by the accretion disc, we adopt a standard Shakura & Sunyaev (1973) disc (see Ghisellini & Tavecchio 2009).

The resulting SEDs and models are shown in Figs A1, A2 and A3, and the model parameters are reported in Tables A1 and A2.

A3 Specific sources

Here, we briefly discuss a few objects for which we do have information on both the BLR and the γ-ray luminosity. These sources lie close to the 'intermediate zone' between BL Lacs and FSRQs. We have constructed their SEDs and modelled them through a simple one-zone leptonic model, as described in Section A2, in order to classify them. With this aim, we adopt the same SED-based classification scheme as discussed in G11 and originally introduced by Padovani & Giommi (1995). In brief, we can classify the object as a FSRQ if the γ-ray luminosity is dominating the electromagnetic output and if the X-ray spectrum is flat (X-ray energy spectral index $\alpha_x < 1$). It is an LBL if the γ-ray luminosity is comparable to the synchrotron one and if $\alpha_x < 1$, and it is an HBL if the γ-ray luminosity is comparable or less than the synchrotron one and $\alpha_x > 1$. Figs A1, A2 and A3 show the SEDs of these sources. We summarize our findings, as follows.

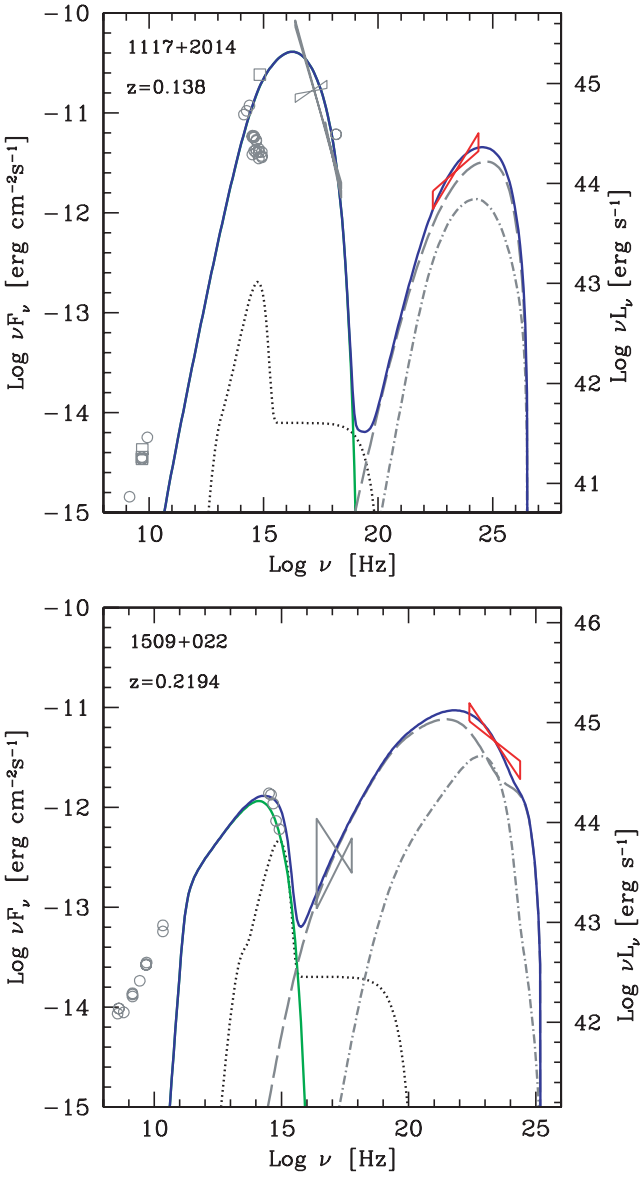

Figure A3. SEDs of 1117+2014 and 1509+022. The lines are the same as in Fig. A1.

Table A2. Logarithm of the jet power in the form of radiation, Poynting flux and the bulk motion of electrons and protons (assuming one proton per emitting electron). Powers are in erg s^{-1}.

Name	log P_r	log P_B	log P_e	log P_p
0937+5008	43.49	42.06	44.47	45.05
1040+23	43.89	43.43	44.08	44.99
1055+01	45.31	44.69	44.68	46.67
1106+023	42.87	41.76	44.58	46.94
1117+2014	42.98	43.66	42.46	42.27
1509+022	44.42	42.04	45.04	46.03

0937+5008

This source is included in the S11 catalogue and it has been detected by *Fermi*. Looking at the SED, it can clearly be classified as a FSRQ, as also suggested from the evident broad Hα and Hβ lines visible in the SDSS spectrum. From the SED modelling, a synchrotron contamination of the optical continuum is visible. Therefore, the automatic estimate of the virial black hole mass performed by S11 could be imprecise. Hence, we have chosen to assign to its black hole an average mass value $M = 5 \times 10^8$ $M_\odot$.

1040+24

This is a *Fermi*-detected source from the SDSS DR6 catalogue, so the black hole mass is not measured. We can assume an average value of $M = 5 \times 10^8$ $M_\odot$. In the SDSS spectrum, a broad Mg II line is clearly visible. From the SED modelling, this source can be classified as an LBL. This means that the thermal continuum can be highly contaminated by the synchrotron emission, although some broad emission lines clearly emerge. Moreover, the disc seems to be only partially covered, and the synchrotron component seems to be very variable. This could result in a variable line EW.

1055+01

This source belongs to the DR6 + 1LAC sample, so the mass is not measured and we assume the average value $M = 5 \times 10^8$ $M_\odot$. As in the case of 1040+24, a broad Mg II line is visible, but it is narrower than the usual broad emission line width (FWHM $\simeq$ 2500 km s^{-1}). This could suggest a small black hole mass, or

Table A1. List of parameters used to construct the theoretical SED. The columns give the following: (1) name; (2) redshift; (3) dissipation radius in units of 10^{15} cm and (in parentheses) in units of Schwarzschild radii; (4) black hole mass in solar masses; (5) the size of the BLR in units of 10^{15} cm; (6) the power injected in the blob calculated in the comoving frame, in units of 10^{45} erg s^{-1}; (7) accretion disc luminosity in units of 10^{45} erg s^{-1} and (in parentheses) in units of L_{Edd}; (8) magnetic field in Gauss; (9) the bulk Lorentz factor at R_{diss}; (10) the viewing angle θ_v in degrees; (11), (12) the break and maximum random Lorentz factors of the injected electrons; (13), (14) the slopes of the injected electron distribution [$Q(\gamma)$] below and above γ_b. The total X-ray corona luminosity is assumed to be in the range of 10–30 per cent of L_d. Its spectral shape is assumed to be always $\propto \nu^{-1}\exp(-h\nu/150\,\mathrm{keV})$.

Name	z	R_{diss}	M	R_{BLR}	P'_i	L_d	B	Γ	θ_v	γ_b	γ_{max}	s_1	s_2
(1)	(2)	(3)	(4)	(5)	(6)	(7)	(8)	(9)	(10)	(11)	(12)	(13)	(14)
0937+5008	0.275	90 (600)	5e8[a]	34.6	2e–3	0.12 (1.6e–3)	0.14	14	3	400	5e3	0	2.5
1040+23	0.56	97.5 (650)	5e8[a]	51.2	1.5e–3	0.26 (3.5e–3)	0.67	13	3	100	9e3	0	2
1055+01	0.888	105 (700)	5e8[a]	98.7	0.02	0.98 (0.013)	3.1	11	3.7	400	9e3	1	2.5
1106+023	0.157	43.2 (3.6e3)	4e7	21.9	3e–3	0.048 (8e–3)	0.22	13	3	6e3	6e3	2	2
1117+2014	0.138	105 (700)	5e8[a]	13.7	5.e–5	0.019 (2.5e–4)	0.7	15	2	3e4	1.5e5	0.5	3
1509+022	0.2194	120 (800)	5e8[a]	34.6	0.022	0.12 (1.6e–3)	0.13	11	6	100	2e4	0	2.3

[a] The mass is assumed.

perhaps the line is partially covered by the continuum and hence the measure is uncertain. The SED does show that the accretion disc contribution is mostly covered by the synchrotron emission. Overall, we can classify this source as a FSRQ, even if the disc emission is dominated by the synchrotron radiation.

1106+023

This is a *Fermi*-detected source from the SDSS DR6 catalogue. In this case, we can estimate its mass with the Chiaberge & Marconi (2011) relation. In fact, the FWHM of its broad Hβ line is reported in the DR6 catalogue. The mass estimate that we obtain is very small ($M = 4 \times 10^7$ M$_\odot$). From the SED, we can see that the disc emerges from the synchrotron component, and hence the emission lines can be seen clearly. From the SED, we can classify this source as an LBL.

1117+2014

This source is present in the S11 catalogue, so it is presumed to be a quasar. However, in the SDSS spectrum, the Hβ line is really faint. Indeed, from the SED modelling, we can classify this source as an HBL. The SED clearly shows that the synchrotron component largely dominates the disc emission, so the automatic estimate of the mass performed by S11 ($M = 4 \times 10^8$ M$_\odot$) is not accurate. Thus, for this source, we assume a value of the black hole equal to the average value.

1509+022

This source is included in the S11 catalogue. Looking at the SED, we can classify it as a FSRQ. However, in this case the continuum also appears to be contaminated by the synchrotron component. Moreover, the S11 results for this source are unclear. The EWs reported in S11 (EW $\sim$ 25–27 Å), do not seem to be recognizable in the spectrum (the lines are hardly visible). Therefore, we think that the S11 estimate of the black hole mass can be considered imprecise, and we replace it with the average value $M = 5 \times 10^8$ M$_\odot$.

This paper has been typeset from a TEX/LATEX file prepared by the author.